Published in final edited form as:
Bone. 2010 May ; 46(5): 1306–1315. doi:10.1016/j.bone.2010.01.380.

Pro416Arg cherubism mutation in *Sh3bp2* knock-in mice affects osteoblasts and alters bone mineral and matrix properties

Chiachien J. Wang[1], **I-Ping Chen**[1], **Boguslawa Koczon-Jaremko**[1], **Adele L. Boskey**[2], **Yasuyoshi Ueki**[3,4], **Liisa Kuhn**[1], and **Ernst J. Reichenberger**[1]

[1]Department of Reconstructive Sciences, School of Dental Medicine, University of Connecticut Health Center, Farmington, CT

[2]Hospital for Special Surgery, New York, NY

[3]Department of Developmental Biology, Harvard School of Dental Medicine, Boston, MA

Abstract

Cherubism is an autosomal dominant disorder in children characterized by unwarranted symmetrical bone resorption of the jaws with fibrous tissue deposition. Mutations causing cherubism have been identified in the adaptor protein SH3BP2. Knock-in mice with a Pro416Arg mutation in *Sh3bp2* exhibit a generalized osteoporotic bone phenotype. In this study, we examined the effects of this "cherubism" mutation on spectroscopic indices of "bone quality" and on osteoblast differentiation. Fourier-transform infrared imaging (FTIRI) analysis of femurs from wild-type and *Sh3bp2* knock-in mice showed decreased mineral content, decreased mineral crystallinity/crystal size, and increased collagen maturity in homozygous mutants. To assess osteoblast maturation *in vivo*, knock-in mice were crossed with transgenic mice over-expressing GFP driven by 3.6-kb or 2.3-kb *Col1a1* promoter fragments. Reduced numbers of mature osteoblasts were observed in homozygous mice. Neonatal calvarial cultures, which were enriched for osteoblasts by depletion of hematopoietic cells (negative selection for Ter119- and CD45-positive cells) were investigated for osteoblast-specific gene expression and differentiation, which demonstrated that differentiation and mineralization in homozygous osteoblast cultures was impaired. Co-cultures with calvarial osteoblasts and bone marrow macrophages showed that mutant osteoblasts appear to increase osteoclastogenesis resulting in increased bone resorption on bone chips. In summary, the *Sh3bp2* mutation in cherubism mice alters bone quality, reduces osteoblast function, and may contribute to excessive bone resorption by osteoclasts. Our data, together with previous osteoclast studies, demonstrate a critical role of *Sh3bp2* in bone remodeling and osteoblast differentiation.

Keywords

cherubism; *Sh3bp2*; osteoblast; GFP transgenic mice; Fourier-transform infrared imaging

Corresponding Author: Ernst Reichenberger, PhD University of Connecticut Health Center (UCHC) Center for Restorative Medicine and Skeletal Development Department of Reconstructive Sciences 263 Farmington Avenue, Farmington, CT 06030-3705 Tel: 860-679-2062 Fax: 860-679-2910 reichenberger@uchc.edu.
[4]current address: Department of Oral Biology, School of Dentistry, University of Missouri-Kansas City

INTRODUCTION

Cherubism is characterized by excessive bilateral bone remodeling restricted to the mandible and maxilla of children and juveniles, leading to multilocular symmetrical cavities. In these patients, the eroded bone is replaced by soft/fibrous tissues. Progressive expansion of this tissue results in a characteristic puffiness of facial features. After puberty, proliferation usually stabilizes and fibrous tissue masses regress over time, but the bone phenotype is still radiographically apparent. There is no standardized treatment for cherubism and surgical intervention may be needed in severe cases.

Previously, studies have identified mutations in the *SH3BP2* adaptor protein as the genetic cause for the autosomal dominant cherubism [1]. To better understand the disease, a knock-in mouse model with a Pro416Arg mutation in *Sh3bp2* (corresponding to Pro418Arg in humans) was generated [2]. Although *Sh3bp2* mutational effects on osteoclasts and inflammatory processes have recently been demonstrated [2,3], their effect on other bone cells, specifically osteoblasts, remains unclear.

Bone homeostasis requires a delicate balance between anabolic osteoblastic and catabolic osteoclastic activities, and impaired osteoblast maturation leads to a diminished capability to generate proper bone as is seen in the case of pathological hypercalcemia, e.g., PTHrP-mediated tumor osteolysis and Vitamin D toxicity [4,5]. Furthermore, the fragile bone in patients with osteogenesis imperfecta, which is clinically characterized by multiple bone fractures from minimum trauma, results from osteoblastic defects that lead to decreased production of functional pro-alpha1(I) and pro-alpha2(I) chains [6]. Maturation of osteoblasts has been extensively studied in well-established *in vitro* culture systems such as calvarial or bone marrow stromal cell cultures [7–10].

Lineage differentiation of normal osteoprogenitors as well as of disease models can be studied with the help of transgenic mice, which express stage-specific *Col1a1*-promoter-driven green fluorescent proteins (GFPs) [7,11,12]. Fragments of the *Col1a1* promoter have been shown to be differentially expressed in various stages of osteoblast development. The 3.6-kb *Col1a1* promoter-driven GFP (pOBCol3.6GFP) was expressed universally in *Col1a1*-producing tissues, including bone, tail tendon, and other non-osseous tissues, while the expression of the 2.3-kb *Col1a1* promoter-driven GFP (pOBCol2.3GFP) was restricted to bone. Histological analysis revealed that osteoblastic cells lining endosteal and trabecular surfaces strongly express pOBCol3.6GFP, in addition to the weaker expression in the fibroblastic cells of the periosteal layer. The pOBCol2.3GFP signal, however, was limited to osteoblasts and osteocytes without detectable signals in periosteal fibroblasts. *In vitro*, pOBCol3.6GFP-positive cells started to appear as spindle-shaped cells before nodule formation and continued to increase signal intensity in cells associated with bone nodules, while pOBCol2.3GFP-positive cells were restricted to mature osteoblasts undergoing mineralization.

In this study, we analyze the skeletal defects of cherubism, specifically the quality of bone, by Fourier-transform infrared imaging (FTIRI). *Sh3bp2* knock-in mice were crossed with transgenic *Col1a1* promoter-driven GFP (pOBCol3.6GFPtpz and pOBCol2.3GFPemd) lines, and the effects of the *Sh3bp2* mutation on osteoblast development is also investigated. In addition, we compare the ability of $Sh3bp2^{KI/KI}$ osteoblasts and wild type osteoblasts to induce functional osteoclasts.

MATERIALS AND METHODS

Animals

Sh3bp2 Pro418Arg knock-in mice were previously generated by homologous recombination [2] as a model for cherubism. The heterozygous (*Sh3bp2*$^{+/KI}$) mice were then cross-bred with mice expressing GFP driven by either 3.6-kb or 2.3-kb *Col1a1* promoter fragments (pOBCol3.6GFPtpz and pOBCol2.3GFPemd, respectively; generously provided by Drs. David Rowe and Peter Maye, UCHC). Mice were housed in the UCHC animal facility and all experiments were approved by the UCHC Animal Care Committee. Mice were genotyped by PCR as described previously [2] and GFP expression was confirmed by UV light excitation.

Tissue preparation, histology, and fluorescent imaging

Ninety-day-old gender-matched mice were used for all analyses. For static histomorphometry, femurs fixed in 4% paraformaldehyde and decalcified in 14% EDTA were sectioned as 5 μm paraffin sections, and stained with hematoxylin for osteoblast surface counting. For *in vivo* GFP analysis, femurs fixed in 4 % paraformaldehyde were transferred to 30% sucrose in PBS over night before embedding in frozen section medium (Richard-Allan Scientific) and flash-freezing using a 2-methylbutane/dry ice bath (Fisher Scientific). Cryosections (5 μm) were produced on a Leica CM3050S Cryostat (Leica Inc, Germany) using a Cryofilm type IIC tape system (FINETEC, Japan). The slides were air dried and kept in dark at −20°C before evaluation. Osteoblast surface, GFP-positive surface, and bone surface were measured in an area 400 μm underneath the growth plate and 200 μm away from cortical bone using OsteoMeasure software (Osteometrics) with microscopy assistance. For fluorescent imaging of GFP signals, slides were submerged in PBS at room temperature, mounted with 50 % glycerin in PBS, and examined with a Zeiss Axioplan 200 inverted microscope equipped with epifluorescence and a Zeiss AxioCam color digital camera (Zeiss, Germany). A composite image was generated from a series of step images using Photoshop. Data were analyzed statistically using the Student t-test (n=6 per group).

Calvarial osteoblast culture

Mouse calvarial osteoblasts (mCOB) were isolated from 5 to 7-day-old postnatal mice by sequential collagenase/trypsin digestion as described previously [11]. Cultures were depleted of hematopoietic cells by negative selection for Ter119-CD45-expressing cells using Dynabeads (Dynal, Invitrogen), and cells were plated at a density of 1.2×10^4 cells/cm^2 in DMEM (Gibco) supplemented with 10 % fetal calf serum (FCS; Hyclone), 100 U/ml of penicillin (Gibco), and 100 μg/ml of streptomycin (Gibco). Cells became confluent 5–7 days after plating and osteoblast differentiation was then initiated by changing to α-MEM (Gibco) (designated day 0 of differentiation) supplemented with 10 % FCS, 50 μg/ml ascorbic acid (Sigma), 4 mM β-glycerophosphate, 100 U/ml of penicillin, and 100 μg/ml of streptomycin (osteoblast differentiation medium). Media was changed every 3 days. To visualize mineral nodule formation, osteoblast cultures were von Kossa stained with 5 % silver nitrate solution while exposed to UV-light for 30 min followed by washing with distilled water. A separate culture was stained with Alizarin red S (AR-S, 40 mM, pH 4.2) for 10 min to determine calcium distribution.

Fourier-transform infrared imaging (FTIRI)

Femurs from 90-day-old gender-matched mice were collected. After removing soft tissues, femurs were fixed in 70 % ethanol and embedded in polymethylmethacrylate (PMMA). Longitudinal non-decalcified sections were cut at 3 μm thickness and sandwiched between two barium fluoride (BaF_2) infrared windows (Spectral Systems) for FTIRI analysis. The FTIR spectra were obtained using a PerkinElmer Spotlight 400 Imaging System (Perkin Elmer

Instruments). A 300×300 μm^2 area in each region of interest (secondary spongiosa and cortex) was examined using a spectral resolution of 16 cm^{-1} and a spatial resolution of ~6.25 μm. Background spectra were collected under identical conditions from the area outside the samples on the same BaF_2 window. The spectra were then zero-corrected for the baseline, normalized, and the spectral contribution of PMMA was subtracted using ISYS Chemical Imaging Software version 5.0 (Spectral Dimensions).

The Perkin-Elmer FTIRI system utilizes a 2×16-array detector attached to an infrared spectrometer to collect multiple spectra simultaneously from selected areas and generates spatially resolved information on the compound of interests. The ratios of mineral to matrix, carbonate to phosphate, as well as crystallinity, and collagen maturity were calculated using the corresponding area or intensity of sub-bands, and the color-coded images of these parameters were displayed. Using ISYS software, IR spectra were converted to generate hyperspectral images (where x and y are the specimen coordinates and z corresponds to infrared band areas) with color intensities representing peak height ratio and integrated area ratios. The following spectroscopic parameters (reviewed in detail by [13]) were calculated: mineral-to-matrix ratio, carbonate-to-phosphate ratio, mineral crystallinity, and collagen crosslink ratio (XLR). The mineral-to-matrix ratio (integrated area ratio of the v_1,v_3 PO_4 band at 916–1180 cm^{-1} and the amide I band at 1585–1720 cm^{-1}) is a measurement that corresponds to ash weight. The carbonate-to-phosphate ratio (integrated area of the v_2 CO_3 band at 840–900 cm^{-1} to the above-mentioned v_1,v_3 PO_4 band) is a measurement that correlates to the aging of mineralized tissues [14,15]. Crystallinity (the intensity ratio of the stoichiometric apatite sub-band at 1030 cm^{-1} and the nonstoichiometric apatite sub-band at 1020 cm^{-1}) is a parameter that reflects both, crystallite size and crystal perfection measured by X-ray diffraction [14]. XLR (the intensity ratio of non-reducible pyridinium cross-link at 1660 cm^{-1} and reducible collagen cross-link at 1690 cm^{-1}) reflects the maturity of collagen matrix [16,17]. Details for spectral processing and validity of the measurements were described elsewhere [14,18]. Over 60 individual points (areas of 25×25 μm measured in point mode) along the center of the bone were recorded for quantification. Each sample was measured twice at the different locations and the average was used to represent individual animals. Student's t-test was used for statistic analysis (n = 6 for *Sh3bp2*$^{+/+}$; n = 5 for *Sh3bp2*$^{KI/KI}$).

Dynamic bone histomorphometry

90-day-old female mice (n = 5 for *Sh3bp2*$^{+/+}$; n = 5 for *Sh3bp2*$^{+/KI}$; n = 7 for *Sh3bp2*$^{KI/KI}$) were intraperitoneally injected with calcein (10 mg/kg body weight) and subsequently with xylenol orange (90 mg/kg body weight) 7 days later. The mice were sacrificed two days after the xylenol orange injection. The femurs from these mice were embedded in OCT medium (Richard-Allan Scientific) and 5μm frozen sections were obtained (Leica cryotome CM3050S). The areas between 400 and 2000 μm distal to the growth plate-metaphyseal junction of the distal femurs were analyzed. The dynamic histomorphometric measurements were obtained using OsteoMeasure software (OsteoMetrics) as described [19].

RNA extraction, cDNA synthesis, and quantitative PCR analysis

Samples were collected on days 0, 7, 14, and 21 after osteoblast differentiation, and RNA was extracted using TRIzol reagent (Invitrogen) according to the manufacturer's protocol. RNA samples were further purified using an RNeasy Mini Kit (Qiagen), and 1 μg of starting RNA was used for cDNA synthesis using ImProm-II reverse-transcriptase (Promega) according to manufacturer's instructions. Quantitative PCR analysis was carried out on an ABI7300 thermocycler (Applied Biosystems) using the iTaq SYBR Green Supermix with ROX (Bio-Rad). Primer designs were generated using the RTPrimerDB database (http://medgen.ugent.be/rtprimerdb/links_menu.php) and concentrations were optimized in separate experiments. 25 ng of cDNA was used per PCR reaction. 3 biological triplicates and

3 technical triplicates were analyzed for each gene. For statistical data processing, we used two-way ANOVA (n=3 for each time point, 4 time points). Bonferroni post-test was used to compare replicate means within specific time points when the genotype effect was significant.

Osteoblast-osteoclast co-culture and bone chip resorption assay

Bovine bone chips were a kind gift from Dr. Joseph Lorenzo (UCHC). Bone chips were stored in 70 % ethanol in −20°C before use. One day before co-culture, calvarial osteoblasts were prepared as above and seeded on the bone chips with a density of 5000 cells/well in 96-well plates. Osteoclast precursors were prepared from bone marrow macrophages (BMM) on a separate plate. Briefly, femurs, tibia, and humeri were cleaned of soft tissues and proximal and distal ends were cut off to flush out bone marrow in DMEM supplemented with 10 % FCS, 100 U/ml of penicillin and 100 μg/ml of streptomycin. After settling overnight, non-adherent cells were collected and subjected to Ficoll purification. BMM of 5000 cells/well were then co-cultured with the previously prepared osteoblasts (5000 cells/well) for 7 days. Half the volume of medium (α-MEM supplemented with 10 % FCS, 50 μg/ml ascorbic acid, 4 mM β-glycerophosphate, 10^{-7}M dexamethasone, 10^{-8} M 1,25$(OH)_2$ vitamin D3, 100 U/ml penicillin and 100 μg/ml streptomycin) was replaced every 3 days. At the end of the culture, cells were fixed and stained for TRAP. For resorption analysis, cells were removed by sonication and bone chips were counterstained with 1 % toluidine blue in 1 % borax buffer to observe resorption pits. 15 random areas on the chip were chosen and the pits were quantified as percent visible area by video area measurement using reflected light microscopy (Boeckler Instruments). Student's t-test was used for statistical analysis (N=15).

RESULTS

Bone chemical and structural analysis

Previous studies of the *Sh3bp2* knock-in mouse model for cherubism reported a general osteoporotic phenotype [2]. To assess the bone quality in cherubism mice, we examined the cortical and trabecular bone at the distal region of femurs from wild type and cherubism *Sh3bp2*$^{KI/KI}$ mice using Fourier-transform infrared imaging (FTIRI) technology to provide further characterization for the chemical composition of bone in cherubism mice.

The *Sh3bp2*$^{KI/KI}$ mice exhibited a significantly lower mineral:matrix ratio compared to their *Sh3bp2*$^{+/+}$ littermates in both cortical and trabecular bone areas (Fig. 1). The *Sh3bp2*$^{+/+}$ and *Sh3bp2*$^{KI/KI}$ cortical bone samples exhibited similar carbonate:phosphate ratios. However, the carbonate:phosphate ratios in cortical bone were statistically higher in comparison to trabecular bone in both, the *Sh3bp2*$^{+/+}$ and *Sh3bp2*$^{KI/KI}$ groups ($p<0.01$). Mineral crystallinity, which correlates to crystal size, was reduced in *Sh3bp2*$^{KI/KI}$ cortical bone. The ratio of collagen crosslinks (XLR) was significantly elevated in trabecular and cortical bone of *Sh3bp2*$^{KI/KI}$ mice.

Bone histomorphometry

Previously, static histomorphometry identified a 3.2-fold increase in osteoblast surfaces in the cherubism *Sh3bp2*$^{KI/KI}$ mice when compared to the *Sh3bp2*$^{+/+}$ littermates [2]. To further assess the level of functional osteoblast activities *in vivo*, femurs from *Sh3bp2*$^{+/+}$, *Sh3bp2*$^{+/KI}$, and *Sh3bp2*$^{KI/KI}$ mice were subjected to dynamic histomorphometric analysis. Unexpectedly, despite the increased osteoblast surface that was determined by a previous static histomorphometric analysis [2], mineral deposition rate and bone formation rate were similar between *Sh3bp2*$^{+/+}$, *Sh3bp2*$^{+/KI}$, and *Sh3bp2*$^{KI/KI}$ mice (Fig. 2). These results indicate that the mutant cherubism *Sh3bp2*$^{KI/KI}$ mice do not display any increased bone formation activity.

To investigate osteoblast differentiation in mutant osteoblasts *in vivo* and *in vitro*, we evaluated femurs of *Sh3bp2*$^{+/KI}$ mice crossed with mice carrying GFP driven by either 3.6-kb or 2.3-kb *Col1a1* promoters (pOBCol3.6GFP or pOBCol2.3GFP). In *Sh3bp2*$^{KI/KI}$/pOBCol3.6GFP^{+} mice, we observed a 3.4-fold increase in the number of GFP-positive cells (Fig. 3). The 3.6-kb *Col1a1* promoter activity is characteristic for pre-/early osteoblasts. However, the number of 2.3-kb GFP-positive cells (marker for mature osteoblasts) decreased ~27 % in the homozygous mutants (*Sh3bp2*$^{KI/KI}$) when compared to *Sh3bp2*$^{+/+}$ littermates. In addition, while there was minimal to no detectable 3.6-kb GFP activity inside cortical bone from wild type mice, we observed abundant 3.6-kb GFP activity in the osteocyte lacunae of the femoral cortex in cherubism mice. These data suggest reduced osteoblast differentiation in the cherubism mouse model.

Osteoblast differentiation

To study osteoblast differentiation on a cellular level, we isolated cells from neonatal calvariae of *Sh3bp2*$^{KI/KI}$/pOBCol3.6GFP^{+} or *Sh3bp2*$^{KI/KI}$/pOBCol2.3GFP^{+} mice by sequential collagenase digestion and differentiated them into osteoblasts. The 3.6-kb *Col1a1* promoter-driven GFP became visible around 5 days of culture and continued to show strong signals in cells associated with bone matrix nodules (Fig. 4). However, no difference in the amount of pOBCol3.6GFP activity was observed between wild type and *Sh3bp2*$^{KI/KI}$ cultures throughout the time course of experiments. Expression of 2.3-kb *Col1a1* promoter-driven GFP in wild type cultures coincided with mineralization of bone matrix nodules. The pOBCol2.3GFP activity in *Sh3bp2*$^{KI/KI}$ cultures, however, was weak compared to expression in *Sh3bp2*$^{+/+}$ cultures at all time points analyzed and never reached the same degree of intensity.

To evaluate whether *Sh3bp2*$^{+/+}$ and *Sh3bp2*$^{KI/KI}$ osteoblasts differentially express bone marker genes, we used quantitative real-time PCR (qPCR) to monitor their temporal expression in culture conditions (Fig. 5). Mouse calvarial osteoblasts used for cultures were depleted of hematopoietic cells by negative selection for Ter119-CD45-positive cells. *Col1a1* and bone sialoprotein (*Bsp*) expression in *Sh3bp2*$^{KI/KI}$ osteoblasts was significantly reduced in cell cultures after 2 weeks in osteogenic medium, respectively. Expression of other osteoblast marker genes (including *Runx2, Alp, Ocn*) were similar between *Sh3bp2*$^{KI/KI}$ and *Sh3bp2*$^{+/+}$ cultures. While there was a tendency for reduced expression of those genes in mature *Sh3bp2*$^{KI/KI}$ osteoblast cultures (day 21 of osteoblast differentiation), the mutation did not affect expression patterns in a statistically significant manner when analyzed by two-way ANOVA. In addition, other markers for bone maturation, such as those associated with mineral deposition, namely von Kossa and Alizarin red S staining, indicated a mild reduction in *Sh3bp2*$^{KI/KI}$ osteoblast activities *in vitro* (Fig. 5F). Together, these data suggest an autonomous negative effect of the *Sh3bp2* mutation on osteoblast differentiation in this mouse model.

Sh3bp2$^{KI/KI}$ osteoblasts enhance osteoclastogenesis through increased Rankl/Opg ratio

Sh3bp2$^{KI/KI}$ mice display hyperactive osteoclast activity with 1.5 to 2-fold increase in osteoclast number per bone surface, as determined by static histomorphometry [2]. However, the mutational effect on the cross-talk between osteoblasts and osteoclasts has previously not been addressed. To test the hypothesis that cherubism *Sh3bp2*$^{KI/KI}$ osteoblasts enhance osteoclastogenesis, we used a co-culture system with either *Sh3bp2*$^{+/+}$ or *Sh3bp2*$^{KI/KI}$ neonatal calvarial osteoblasts and bone marrow macrophage (BMM)-derived osteoclasts from *Sh3bp2*$^{+/+}$ mice (Fig. 6). Osteoblasts were depleted of hematopoietic cells prior to co-culture by negative selection with Dynabeads and CD 45 and Ter119 antibodies. *Sh3bp2*$^{KI/KI}$ osteoblasts generated almost twice the amount of TRAP-positive cells when compared to *Sh3bp2*$^{+/+}$ osteoblasts (Fig. 6A). Bone resorption assays with *Sh3bp2*$^{KI/KI}$ osteoclasts cultured on bovine bone chips resulted in resorption areas that were 36 % increased compared to resorption areas of *Sh3bp2*$^{+/+}$ cultures (Fig. 6B).

We used qPCR to evaluate gene expression during osteoclastogenesis investigate events that lead to the enhancement of osteoclastogenesis by *Sh3bp2*$^{KI/KI}$ osteoblasts (Fig. 6C–F). At day 7 of osteoblastic differentiation, *Sh3bp2*$^{KI/KI}$ osteoblasts showed a 150 % increase in *Rankl* expression by qPCR (Fig. 6C), while osteoprotegerin (*Opg*) was reduced by 60% compared to *Sh3bp2*$^{+/+}$ osteoblasts (Fig. 6D). Furthermore, the *Rankl*/*Opg* ratio at day 7 of osteoblastic differentiation was 2.4-fold higher in *Sh3bp2*$^{KI/KI}$ osteoblast cultures compared to *Sh3bp2*$^{+/+}$ cultures (Fig. 6E). Therefore, we conclude that an increased RANKL/OPG ratio may contribute in part to enhanced osteoclastogenesis in *Sh3bp2*$^{KI/KI}$ mice. To investigate whether the mutation in *Sh3bp2* affected osteoblast through TNF-α in an autocrine manner, the gene expression level of *Tnf*-α in *Sh3bp2*$^{KI/KI}$ osteoblasts was analyzed by qPCR (Fig. 6F). While the levels of *Tnf*-α expression were comparable at the day 0 of the culture, the level increased in the *Sh3bp2*$^{+/+}$ osteoblasts while the level remained low in the *Sh3bp2*$^{KI/KI}$ osteoblasts.

DISCUSSION

Structural properties of bone in animal models for human diseases are frequently studied by histomorphometry or micro-computed tomography (μ-CT), but material properties of bone remain as one of the less researched elements of bone quality. Vibrational spectroscopy, such as FTIR, has been used to characterize pathological calcification and developmental change in bone and other mineralized tissues [18,20–23]. The material properties that contribute to bone strength include, *inter alia*, mineral content, mineral composition, mineral crystallinity, and matrix composition and cross-linking. Changes of these parameters in bone diseases such as osteogenesis imperfecta [24], osteopetrosis [25], osteomalacia [26], and osteoporosis [22, 27] have been characterized using FTIR and FTIRI.

Previous μ-CT studies had shown that *Sh3bp2*$^{KI/KI}$ mice displayed an overall bone deficit, which has been attributed to increased osteoclast activity [2] and therefore the possibility of high bone turnover had been considered. However, although an increased osteoblast surface was shown in these mice compared to their wild-type littermates [2], the authors did not show increased bone formation activities by dynamic histomorphometry. Therefore, the question remained whether the osteoporotic phenotype in *Sh3bp2*$^{KI/KI}$ mice is due to increased bone resorption alone or high bone turnover in general. Indeed, our dynamic histomorphometry showed that mineral apposition rate and bone formation rates between mutant and wild type mice were not significantly different, suggesting that the *Sh3bp2*$^{KI/KI}$ model is not a high bone turnover model.

We hypothesized that the bone deficit phenotype in *Sh3bp2*$^{KI/KI}$ mice may be due in part to deposition of abnormal bone matrix by osteoblasts. Our calvarial osteoblast cultures from *Sh3bp2*$^{KI/KI}$ mice showed reduced *in vitro* mineralization activity as compared to *Sh3bp2*$^{+/+}$ cultures by von Kossa staining. However, it is well known that von Kossa staining alone is not sufficient to differentiate cell-mediated bone-like mineralization from dystrophic precipitation of mineral [28,29]. The clear association of mineral with the 2.3-kb *Col1a1* promoter-driven GFP in the cell cultures confirmed that the mineral deposition was linked to mature osteoblasts, was formed in bone matrix nodules and was not dystrophic. The reduced von Kossa staining correlates to the weaker pOBCol2.3GFP activity in *Sh3bp2*$^{KI/KI}$ cultures. This finding of reduced mineralization and reduced pOBCol2.3GFP activity *in vitro* is consistent with our *in vivo* studies. The observation of increased osteoid formation in bone of *Sh3bp2*$^{KI/KI}$ mice [30] is further consistent with undermineralized bone matrix in this model.

Analysis of femoral bone from *Sh3bp2*$^{KI/KI}$ mice by FTIR revealed reduced mineral content, reduced mineral crystallinity/size, and normal mineral maturation with increased collagen crosslinking. Studies from patients and animal models with osteoporosis demonstrated that

reduced mineral-to-matrix ratio correlates to decreased ash weight [22,27]. In *Sh3bp2*$^{KI/KI}$ mice, the significant decrease in mineral:matrix ratio is consistent with the general osteoporotic phenotype previously observed by μ-CT analysis [2].

Crystal size and perfection of hydroxyapatite in cortical bone was slightly but significantly reduced in *Sh3bp2*$^{KI/KI}$ mice, a finding that corresponds to the reduced number of mature, matrix depositing osteoblasts in cortical bone shown in the histological images showing *Col1a1* promoter-driven GFP activity. It is possible that the decreased expression of bone sialoprotein, which binds to calcium and hydroxyapatite through its acidic amino acid cluster, contributes to the reduced crystal size and reduced mineral content in the matured bone matrix in *Sh3bp2*$^{KI/KI}$ mice. Reduced average crystal size measured by XRD has been reported in bones of osteoporosis patients [31,32] although there are other reports of increased crystal size most likely due to the reduction of the trabecular bone component in osteoporotic patients [33–35], and has been observed in animal models (Tgf-β1 knock-out mice) with reduced osteoblast proliferation and matrix maturation that affects bone quality [36]. Cortical bone mineral is typically more mature than trabecular bone mineral, with increased crystal size and an increased carbonate:phosphate ratio, due to reduced turnover in cortical bone [37]. This was found to be true in the present study implying that normal maturation processes are occurring in the mineral that is deposited, but that fewer and smaller crystals are deposited initially in the *Sh3bp2*$^{KI/KI}$ mice as compared to the wild type.

Sh3bp2$^{KI/KI}$ mice demonstrated elevated collagen cross-linking levels in trabecular and cortical bone. Recent studies found that osteoporosis patients have increased as well as different distribution of collagen cross-linking [38]. The change in this index and the pattern of collagen maturity relative to healthy individuals may contribute to bone fragility. These authors suggested that matrix might mature faster because of reduced mineralization in osteoporotic bone and therefore, show increased levels of non-reducible pyridinium crosslinks. We interpret our results as another indication that the bone matrix produced in osteoporosis is different from normal bone matrix although we cannot disregard a possible imbalance in crosslinking enzymes that leads to increased non-reducible crosslinking. It is more likely, however, that alterations in the organic bone matrix contribute to the enhanced rate of pyridinium crosslinking.

Sh3bp2 was first identified as a binding partner for the proto-oncogene *c-Abl* [39]. *c-Abl* knockout mice develop an osteoporosis phenotype due to osteoblast-specific impairments [40]. It is conceivable that the alteration of bone mineralization and maturity is in part a function of cell-autonomous effects of the *Sh3bp2* mutation in osteoblasts. Indeed, osteoblasts from *Sh3bp2*$^{KI/KI}$ mice appeared to diverge in their differentiation properties in our *in vivo* differentiation analysis. *Col1a1* promoter-driven transgenic GFP markers have been shown to characterize osteoblast lineage progression [11,12] in various animal models. 3.6-kb *Col1a1* GFP activity represents an early osteoblast differentiation status (and is also expressed in other collagen type I expressing cells) while 2.3-kb *Col1a1* GFP activity is characteristic for mature osteoblasts. *Sh3bp2*$^{KI/KI}$ mice showed 27% less pOBCol2.3GFP activity despite the increased number of pOBCol3.6GFP^{+} cells, which suggests that the number of mature osteoblasts is decreased. At the same time, we saw pOBCol3.6GFP expression on the bone lining surface of trabecular bone of *Sh3bp2*$^{KI/KI}$ mice increase 3.4-fold in experiments where the amount of measured GFP signals was normalized to the bone surface. The increased 3.6-kb *Col1a1* promoter activity indicates an abundance of immature osteoblasts failing to reach their terminal differentiation stage. It has been shown that the 3.6-kb fragment of the *Col1a1* promoter can drive expression in both, osteoblast and osteoclast lineage cells *in vivo* [41]. Since cystic lesions in cherubism mice are rich in cells of myeloid lineage and osteoclasts, we cannot exclude that osteoclasts on the bone surface also contribute to the pOBCol3.6GFP activity. However, the

number of osteoclasts on the bone surface represents only a small fraction of the osteoblast lineage cells and would not alter the analysis in a noticeable manner.

These *in vivo* results were confirmed by *in vitro* studies, where calvarial osteoblast cultures from *Sh3bp2*$^{KI/KI}$ mice showed a remarkable decrease in 2.3-kb *Col1a1* GFP activity. In the time course of the experiments, the pOBCol2.3GFP activity in *Sh3bp2*$^{KI/KI}$ osteoblasts never reached the same level as in *Sh3bp2*$^{+/+}$ osteoblasts suggesting a defect in differentiation/maturation instead of delayed maturity. However, we found no noticeable change of 3.6-kb *Col1a1* GFP expression under our experimental conditions. It has been shown that *Sh3bp2* is required for the progression of pre-B cells to B cells [42] and it could be possible that *Sh3bp2* may play a similar role in other cellular lineages, such as osteoblast precursors. We propose that a mutational defect in *Sh3bp2* blocks the progression of early osteoblasts *in vivo* and leads to increased numbers of 3.6-kb *Col1a1* GFP-positive cells. The discrepancy between 3.6-kb *Col1a1* GFP activity in cultured calvarial osteoblasts and *in vivo* data may be due to a limitation of the cell culture system.

Because bone of *Sh3bp2*$^{KI/KI}$ mice could potentially contain erosive bone lesions filled with inflammatory cells of myeloid lineage, we enriched cultures for mesenchymal cell populations by negative selection for hematopoietic cells expressing CD45 and Ter119 before primary cell plating to remove potential hematopoietic subpopulations. Such inflammatory infiltrates (described in [2]) can be found in long bone or in cranial bone of cherubism mice. We realize that with this method we may not have eliminated stem cells or early hematopoietic progenitors, which could give rise to a skewed composition of cells in culture. However, FACS analysis with cells after negative selection that had been cultured in osteogenic medium for 2-weeks, did not show an increased number of hematopoietic cells (data not shown). We are therefore convinced that the described GFP expression patterns in osteogenic cultures are due to expression in mesenchymal cells. We conclude that osteoblast maturation in *Sh3bp2*$^{KI/KI}$ mice is reduced, which may lead to the failure to lay down bone of adequate quality.

The *Sh3bp2* mutation appears to have cell-autonomous effects on osteoclasts (resulting in increased osteoclast number and activity *in vivo*) and on osteoblasts (impaired mineral and matrix deposition and osteoblast maturation). Therefore, the effect on bone turnover rate from the cross-talk between osteoblasts and osteoclasts needs to be considered as well. Our data demonstrate that *Sh3bp2*$^{KI/KI}$ osteoblasts directly enhance osteoclastogenesis by increasing the *Rankl*/*Opg* ratio. The imbalanced coupling of osteoblasts and osteoclasts was confirmed in co-culture studies by increased multinuclear TRAP-positive cells and increased resorption pit areas when *Sh3bp2*$^{KI/KI}$ osteoblasts were cultured with *Sh3bp2*$^{+/+}$ osteoclasts. The reduced level of osteoblast maturation in *Sh3bp2*$^{KI/KI}$ mice may contribute to increased amounts of osteoclasts as less mature osteoblasts may result in increased osteoclastogenesis [43,44]. On the other hand, there is evidence that the presence of inflammation in (arthritic) bone may impair formation of adequately mineralized bone [45]. TNF-alpha levels in serum of *Sh3bp2*$^{KI/KI}$ mice is significantly increased [2] and it is known that TNF-α can inhibit osteoblast differentiation [46]. However, in our *in vitro* calvarial osteoblast culture system, *Sh3bp2*$^{KI/KI}$ osteoblasts expressed reduced levels of *Tnf*-α message compared to *Sh3bp2*$^{+/+}$ osteoblasts. While inhibition of osteoblast differentiation by TNF-α may explain some of our *in vivo* findings, it does not explain the reduced osteoblast differentiation potential *in vitro*.

In summary, our studies showed that the cherubism mutation in *Sh3bp2* has previously unrecognized effects on osteoblasts. Although increased osteoblast surfaces were observed in cherubism mice, the bone formation activity did not increase. Instead, the osteoblasts in cherubism mice appeared to be immature and to deposit defective bone matrix. The mutational effect of *Sh3bp2* in cherubism may result in differentiating osteoblasts reaching mature status at a lesser rate, which may contribute to abnormal matrix deposition and exacerbate the negative

bone mass balance. Due to the increase of *Rankl*/*Opg* ratio in cultured cells, we believe that mutant osteoblasts can further enhance osteoclastogenesis and therefore contribute to the unbalanced bone remodeling in cherubism in addition to the previously identified TNF-α mediated mechanism.

Acknowledgments

We would like to thank Drs. David Rowe and Peter Maye for providing GFP transgenic mice and assisting with fluorescent microscopy, the UCHC Histomorphometry Core for use of their facility, and Dr. Joseph Lorenzo for providing bone chips. We wish to thank the Bone Group at UCHC for their helpful discussions. CJW was supported by NIH T32 training grant DE007302 and AB's efforts were supported by AR037661 and AR046121. YU was supported by Charles H. Hood Foundation, Inc., Boston, MA. The project was supported by institutional funding to EJR.

REFERENCES

[1]. Ueki Y, Tiziani V, Santanna C, Fukai N, Maulik C, Garfinkle J, Ninomiya C, doAmaral C, Peters H, Habal M, Rhee-Morris L, Doss JB, Kreiborg S, Olsen BR, Reichenberger E. Mutations in the gene encoding c-Abl-binding protein SH3BP2 cause cherubism. Nat Genet 2001;28:125–6. [PubMed: 11381256]

[2]. Ueki Y, Lin CY, Senoo M, Ebihara T, Agata N, Onji M, Saheki Y, Kawai T, Mukherjee PM, Reichenberger E, Olsen BR. Increased Myeloid Cell Responses to M-CSF and RANKL Cause Bone Loss and Inflammation in SH3BP2 “Cherubism” Mice. Cell 2007;128:71–83. [PubMed: 17218256]

[3]. Aliprantis AO, Ueki Y, Sulyanto R, Park A, Sigrist KS, Sharma SM, Ostrowski MC, Olsen BR, Glimcher LH. NFATc1 in mice represses osteoprotegerin during osteoclastogenesis and dissociates systemic osteopenia from inflammation in cherubism. J Clin Invest 2008;118:3775–89. [PubMed: 18846253]

[4]. Juraschek M, Seibel MJ, Woitge HW, Krempien B, Bauss F. Association between histomorphometry and biochemical markers of bone turnover in a longitudinal rat model of parathyroid hormone-related peptide (PTHrP)-mediated tumor osteolysis. Bone 2000;26:475–83. [PubMed: 10773587]

[5]. Wronski TJ, Halloran BP, Bikle DD, Globus RK, Morey-Holton ER. Chronic administration of 1,25-dihydroxyvitamin D3: increased bone but impaired mineralization. Endocrinology 1986;119:2580–5. [PubMed: 3780540]

[6]. Shapiro JR, McBride DJ Jr. Fedarko NS. OIM and related animal models of osteogenesis imperfecta. Connect Tissue Res 1995;31:265–8. [PubMed: 15612365]

[7]. Kalajzic I, Staal A, Yang WP, Wu Y, Johnson SE, Feyen JH, Krueger W, Maye P, Yu F, Zhao Y, Kuo L, Gupta RR, Achenie LE, Wang HW, Shin DG, Rowe DW. Expression profile of osteoblast lineage at defined stages of diferentiation. J Biol Chem. 2005

[8]. Dacic S, Kalajzic I, Visnjic D, Lichtler AC, Rowe DW. Col1a1-driven transgenic markers of osteoblast lineage progression. J Bone Miner Res 2001;16:1228–36. [PubMed: 11450698]

[9]. Beresford JN, Graves SE, Smoothy CA. Formation of mineralized nodules by bone derived cells in vitro: a model of bone formation? Am J Med Genet 1993;45:163–78. [PubMed: 8456798]

[10]. Siggelkow H, Rebenstorff K, Kurre W, Niedhart C, Engel I, Schulz H, Atkinson MJ, Hufner M. Development of the osteoblast phenotype in primary human osteoblasts in culture: comparison with rat calvarial cells in osteoblast differentiation. J Cell Biochem 1999;75:22–35. [PubMed: 10462701]

[11]. Kalajzic I, Kalajzic Z, Kaliterna M, Gronowicz G, Clark SH, Lichtler AC, Rowe D. Use of type I collagen green fluorescent protein transgenes to identify subpopulations of cells at different stages of the osteoblast lineage. J Bone Miner Res 2002;17:15–25. [PubMed: 11771662]

[12]. Jiang X, Kalajzic Z, Maye P, Braut A, Bellizzi J, Mina M, Rowe DW. Histological analysis of GFP expression in murine bone. J Histochem Cytochem 2005;53:593–602. [PubMed: 15872052]

[13]. Gourion-Arsiquaud S, West PA, Boskey AL. Fourier transform-infrared microspectroscopy and microscopic imaging. Methods Mol Biol 2008;455:293–303. [PubMed: 18463826]

[14]. Gadaleta SJ, Landis WJ, Boskey AL, Mendelsohn R. Polarized FT-IR microscopy of calcified turkey leg tendon. Connect Tissue Res 1996;34:203–11. [PubMed: 9023049]

[15]. Ou-Yang H, Paschalis EP, Mayo WE, Boskey AL, Mendelsohn R. Infrared microscopic imaging of bone: spatial distribution of CO3(2-). J Bone Miner Res 2001;16:893–900. [PubMed: 11341334]

[16]. Paschalis EP, Verdelis K, Doty SB, Boskey AL, Mendelsohn R, Yamauchi M. Spectroscopic characterization of collagen cross-links in bone. J Bone Miner Res 2001;16:1821–8. [PubMed: 11585346]

[17]. Blank RD, Baldini TH, Kaufman M, Bailey S, Gupta R, Yershov Y, Boskey AL, Coppersmith SN, Demant P, Paschalis EP. Spectroscopically determined collagen Pyr/deH-DHLNL cross-link ratio and crystallinity indices differ markedly in recombinant congenic mice with divergent calculated bone tissue strength. Connect Tissue Res 2003;44:134–42. [PubMed: 14504033]

[18]. Boskey A, Pleshko Camacho N. FT-IR imaging of native and tissue-engineered bone and cartilage. Biomaterials 2007;28:2465–78. [PubMed: 17175021]

[19]. Parfitt AM, Drezner MK, Glorieux FH, Kanis JA, Malluche H, Meunier PJ, Ott SM, Recker RR. Bone histomorphometry: standardization of nomenclature, symbols, and units. Report of the ASBMR Histomorphometry Nomenclature Committee. J Bone Miner Res 1987;2:595–610. [PubMed: 3455637]

[20]. Mayer-Kuckuk P, Boskey AL. Molecular imaging promotes progress in orthopedic research. Bone 2006;39:965–77. [PubMed: 16843078]

[21]. Boskey A, Mendelsohn R. Infrared analysis of bone in health and disease. J Biomed Opt 2005;10:031102. [PubMed: 16229627]

[22]. Boskey AL, DiCarlo E, Paschalis E, West P, Mendelsohn R. Comparison of mineral quality and quantity in iliac crest biopsies from high- and low-turnover osteoporosis: an FT-IR microspectroscopic investigation. Osteoporos Int 2005;16:2031–8. [PubMed: 16088360]

[23]. Verdelis K, Lukashova L, Yamauchi M, Atsawasuwan P, Wright JT, Peterson MG, Jha D, Boskey AL. Changes in matrix phosphorylation during bovine dentin development. Eur J Oral Sci 2007;115:296–302. [PubMed: 17697169]

[24]. Camacho NP, Landis WJ, Boskey AL. Mineral changes in a mouse model of osteogenesis imperfecta detected by Fourier transform infrared microscopy. Connect Tissue Res 1996;35:259–65. [PubMed: 9084664]

[25]. Boskey A. Mineral changes in osteopetrosis. Crit Rev Eukaryot Gene Expr 2003;13:109–16. [PubMed: 14696960]

[26]. Faibish D, Gomes A, Boivin G, Binderman I, Boskey A. Infrared imaging of calcified tissue in bone biopsies from adults with osteomalacia. Bone 2005;36:6–12. [PubMed: 15663997]

[27]. Faibish D, Ott SM, Boskey AL. Mineral changes in osteoporosis: a review. Clin Orthop Relat Res 2006;443:28–38. [PubMed: 16462423]

[28]. Gronowicz G, Woodiel FN, McCarthy MB, Raisz LG. In vitro mineralization of fetal rat parietal bones in defined serum-free medium: effect of beta-glycerol phosphate. J Bone Miner Res 1989;4:313–24. [PubMed: 2763870]

[29]. Bonewald LF, Harris SE, Rosser J, Dallas MR, Dallas SL, Camacho NP, Boyan B, Boskey A. von Kossa staining alone is not sufficient to confirm that mineralization in vitro represents bone formation. Calcif Tissue Int 2003;72:537–47. [PubMed: 12724828]

[30]. Mukherjee PM, Wang CJ, Chen I-P, Koczon-Jaremko B, Olsen BR, Ueki Y, Reichenberger E. Cherubism Gene Sh3bp2 is Important for Optimal Bone Formation, Osteoblast Differentiation and Function. AJODO. 2010 accepted for publication.

[31]. Grynpas MD, Holmyard D. Changes in quality of bone mineral on aging and in disease. Scanning Microsc 1988;2:1045–54. [PubMed: 3399845]

[32]. Sastry TP, Chandrsekaran A, Sundaraseelan J, Ramasastry M, Sreedhar R. Comparative study of some physico-chemical characteristics of osteoporotic and normal human femur heads. Clin Biochem 2007;40:907–12. [PubMed: 17512512]

[33]. Paschalis EP, Glass EV, Donley DW, Eriksen EF. Bone mineral and collagen quality in iliac crest biopsies of patients given teriparatide: new results from the fracture prevention trial. J Clin Endocrinol Metab 2005;90:4644–9. [PubMed: 15914535]

[34]. Durchschlag E, Paschalis EP, Zoehrer R, Roschger P, Fratzl P, Recker R, Phipps R, Klaushofer K. Bone material properties in trabecular bone from human iliac crest biopsies after 3- and 5-year treatment with risedronate. J Bone Miner Res 2006;21:1581–90. [PubMed: 16995813]

[35]. Gourion-Arsiquaud S, Faibish D, Myers E, Spevak L, Compston J, Hodsman A, Shane E, Recker RR, Boskey ER, Boskey AL. Use of FTIR spectroscopic imaging to identify parameters associated with fragility fracture. J Bone Miner Res 2009;24:1565–71. [PubMed: 19419303]

[36]. Atti E, Gomez S, Wahl SM, Mendelsohn R, Paschalis E, Boskey AL. Effects of transforming growth factor-beta deficiency on bone development: a Fourier transform-infrared imaging analysis. Bone 2002;31:675–84. [PubMed: 12531561]

[37]. Kuhn LT, Grynpas MD, Rey CC, Wu Y, Ackerman JL, Glimcher MJ. A comparison of the physical and chemical differences between cancellous and cortical bovine bone mineral at two ages. Calcif Tissue Int 2008;83:146–54. [PubMed: 18685796]

[38]. Paschalis EP, Shane E, Lyritis G, Skarantavos G, Mendelsohn R, Boskey AL. Bone fragility and collagen cross-links. J Bone Miner Res 2004;19:2000–4. [PubMed: 15537443]

[39]. Ren R, Mayer BJ, Cicchetti P, Baltimore D. Identification of a ten-amino acid proline-rich SH3 binding site. Science 1993;259:1157–61. [PubMed: 8438166]

[40]. Li BBS, de los Santos K, Schieren I, Quiroz M, Teitelbaum SL, Tondravi MM, Goff SP. Mice deficient in Abl are osteoporotic and have defects in osteoblast maturation. Nat Genet 2000;24:304–8. [PubMed: 10700189]

[41]. Boban I, Jacquin C, Prior K, Barisic-Dujmovic T, Maye P, Clark SH, Aguila HL. The 3.6 kb DNA fragment from the rat Col1a1 gene promoter drives the expression of genes in both osteoblast and osteoclast lineage cells. Bone 2006;39:1302–12. [PubMed: 16938497]

[42]. de la Fuente MA, Kumar L, Lu B, Geha RS. 3BP2 deficiency impairs the response of B cells, but not T cells, to antigen receptor ligation. Mol Cell Biol 2006;26:5214–25. [PubMed: 16809760]

[43]. Thomas GP, Baker SU, Eisman JA, Gardiner EM. Changing RANKL/OPG mRNA expression in differentiating murine primary osteoblasts. J Endocrinol 2001;170:451–60. [PubMed: 11479141]

[44]. Atkins GJ, Kostakis P, Pan B, Farrugia A, Gronthos S, Evdokiou A, Harrison K, Findlay DM, Zannettino AC. RANKL expression is related to the differentiation state of human osteoblasts. J Bone Miner Res 2003;18:1088–98. [PubMed: 12817763]

[45]. Walsh NC, Reinwald S, Manning CA, Condon KW, Iwata K, Burr DB, Gravallese EM. Osteoblast function is compromised at sites of focal bone erosion in inflammatory arthritis. J Bone Miner Res 2009;24:1572–85. [PubMed: 19338457]

[46]. Gilbert L, He X, Farmer P, Boden S, Kozlowski M, Rubin J, Nanes MS. Inhibition of osteoblast differentiation by tumor necrosis factor-alpha. Endocrinology 2000;141:3956–64. [PubMed: 11089525]

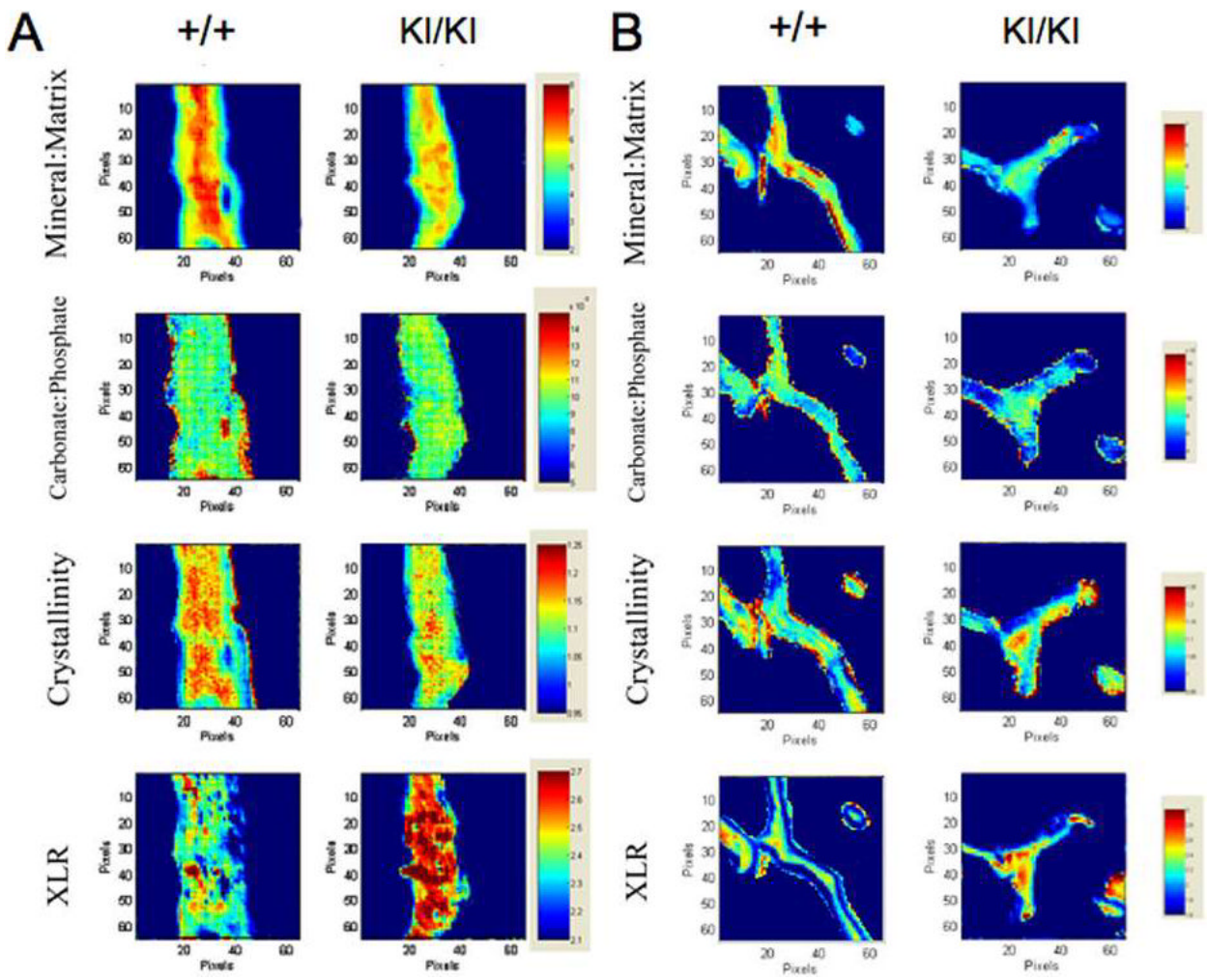

Fig. 1.

Fourier-transform infrared imaging (FTIRI) of wild-type (*Sh3bp2*$^{+/+}$) and *Sh3bp2* knock-in (*Sh3bp2*$^{KI/KI}$) mice showing representative infrared images of cortical bone (A) and trabecular bone (B). Each image represents a 400×400 um area with 6.25 μm spatial resolution. The numerical color scales represent the range of intensity ratio for each parameter and were adjusted to be constant among samples.

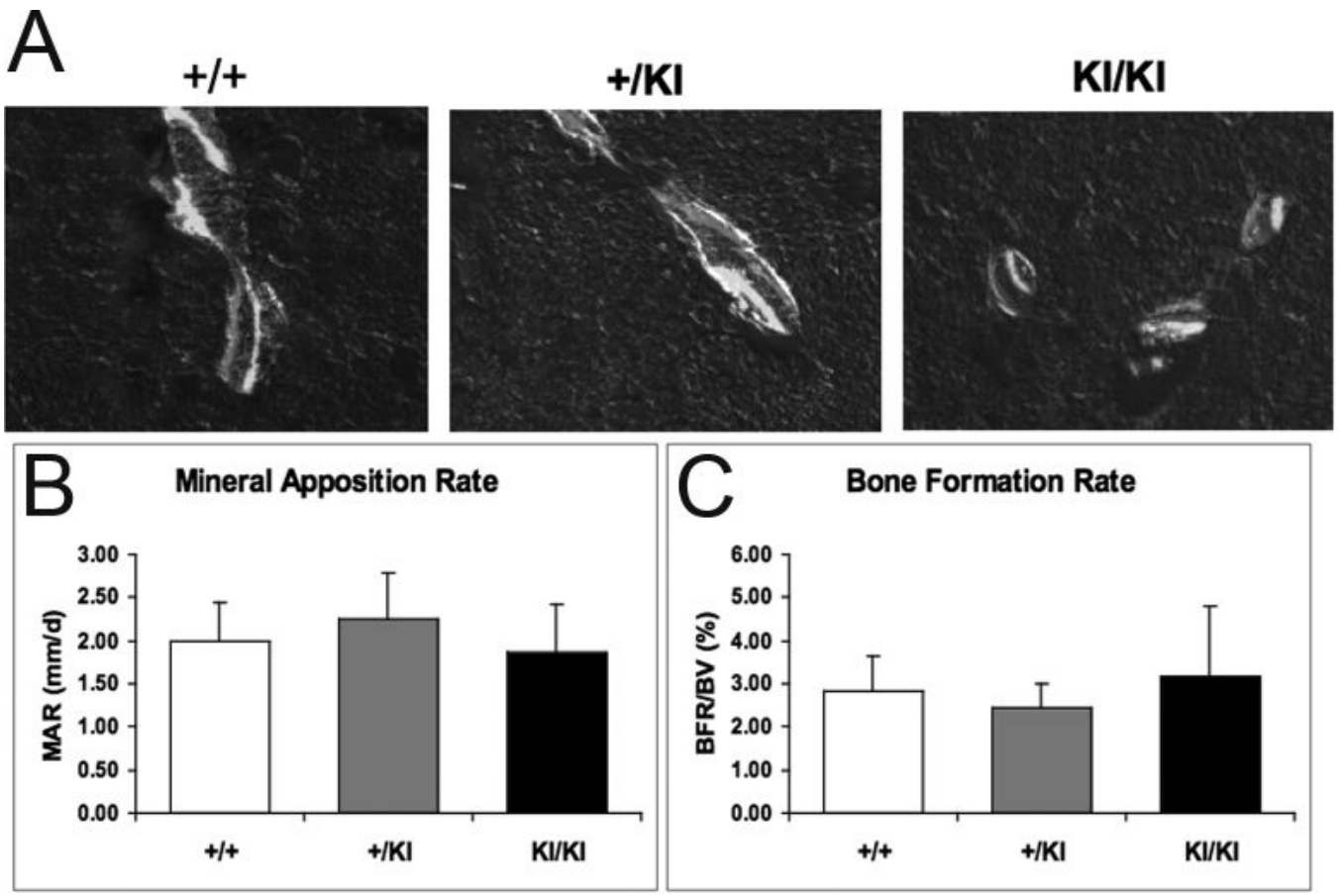

Fig. 2.

Dynamic histomorphometric analysis of *Sh3bp2*$^{+/+}$, *Sh3bp2*$^{+/KI}$, and *Sh3bp2*$^{KI/KI}$ mice. Double labels of calcein (green) and xylenol orange (red) were sequentially injected to 90-day-old mice to assess bone formation activities. Representative images from trabecular bones are shown (A). Mineral deposition rate (B) and bone formation rate (C) were similar between *Sh3bp2*$^{+/+}$, *Sh3bp2*$^{+/KI}$, and *Sh3bp2*$^{KI/KI}$ mice. (Student's t-test; n = 5 for *Sh3bp2*$^{+/+}$; n = 5 for *Sh3bp2*$^{+/KI}$; n = 7 for *Sh3bp2*$^{KI/KI}$).

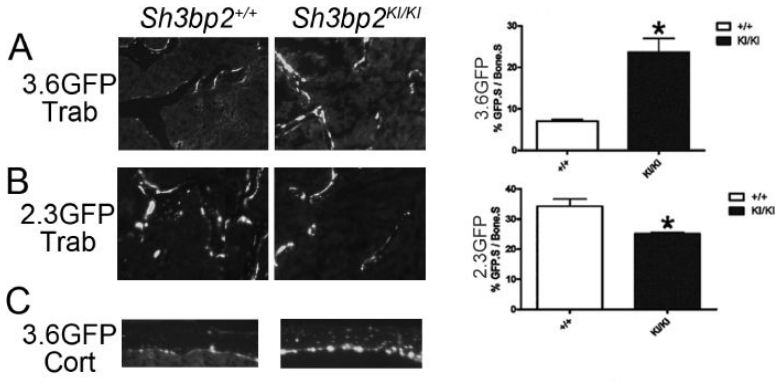

Fig. 3.

In vivo monitoring of cherubism *Sh3bp2*$^{KI/KI}$ osteoblast cultures using *Col1a1* promoter-driven GFP. *Sh3bp2*$^{+/+}$ and *Sh3bp2*$^{KI/KI}$ mice were crossed with transgenic mice overexpressing GFP driven by either 3.6-kb or 2.3-kb *Col1a1* promoters. Frozen sections (5 μm) of femurs from 10-week-old mice showed increased numbers of 3.6-kb *Col1a1* GFP positive cells (3.6GFP) in *Sh3bp2*$^{KI/KI}$ mice (A), but decreased numbers of 2.3-kb *Col1a1* GFP positive cells (2.3GFP) (B). (Student's t-test; n=6 for pOBCol3.6GFPtpz; n=4 for pOBCol2.3GFPemd, *p<0.05). 3.6-kb Col1a1 promoter in osteocytes from femoral cortex of *Sh3bp2*$^{KI/KI}$ but not of *Sh3bp2*$^{+/+}$ mice was active (C). Trab: trabecular bone. Cort: Cortical bone.

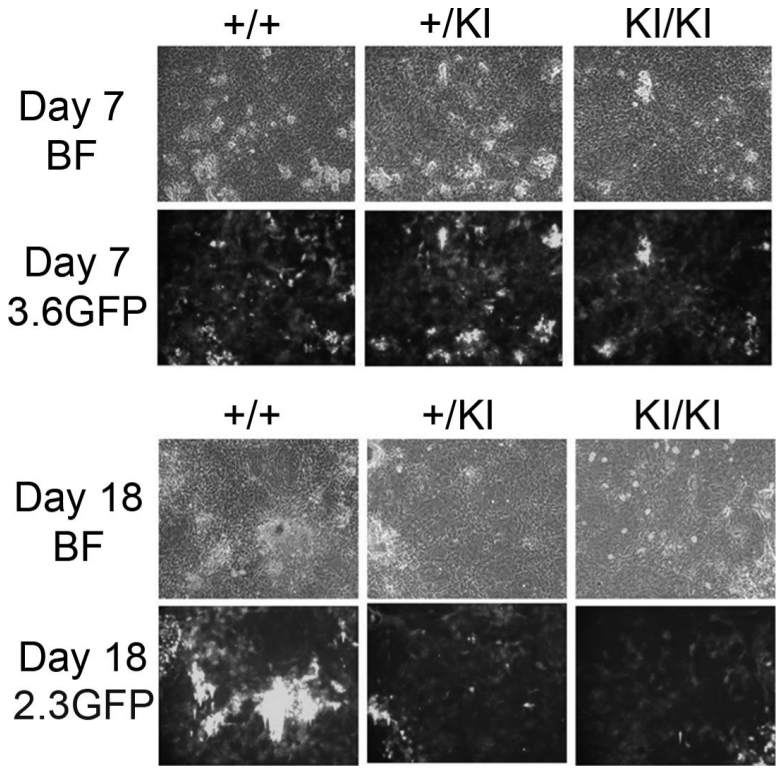

Fig. 4.

pOBCol3.6GFPtpz and pOBCol2.3GFPemd expression in calvarial cell cultures. Calvarial osteoblasts with GFP driven by a 3.6-kb Col1a1 promoter (pOBCol3.6GFPtpz) from *Sh3bp2*$^{+/+}$, *Sh3bp2*$^{+/KI}$, and *Sh3bp2*$^{KI/KI}$ mice showed no difference in GFP activity on day 7 of osteoblast differentiation (A); Calvarial osteoblasts with GFP driven by a 2.3-kb Col1a1 promoter (pOBCol2.3GFPemd) from *Sh3bp2*$^{KI/KI}$ mice showed reduced GFP activity compared to *Sh3bp2*$^{+/+}$ samples on day 18 of osteoblast differentiation (B). BF: bright field; 3.6GFP: GFPtpz filter; 2.3GFP: GFPemd filter.

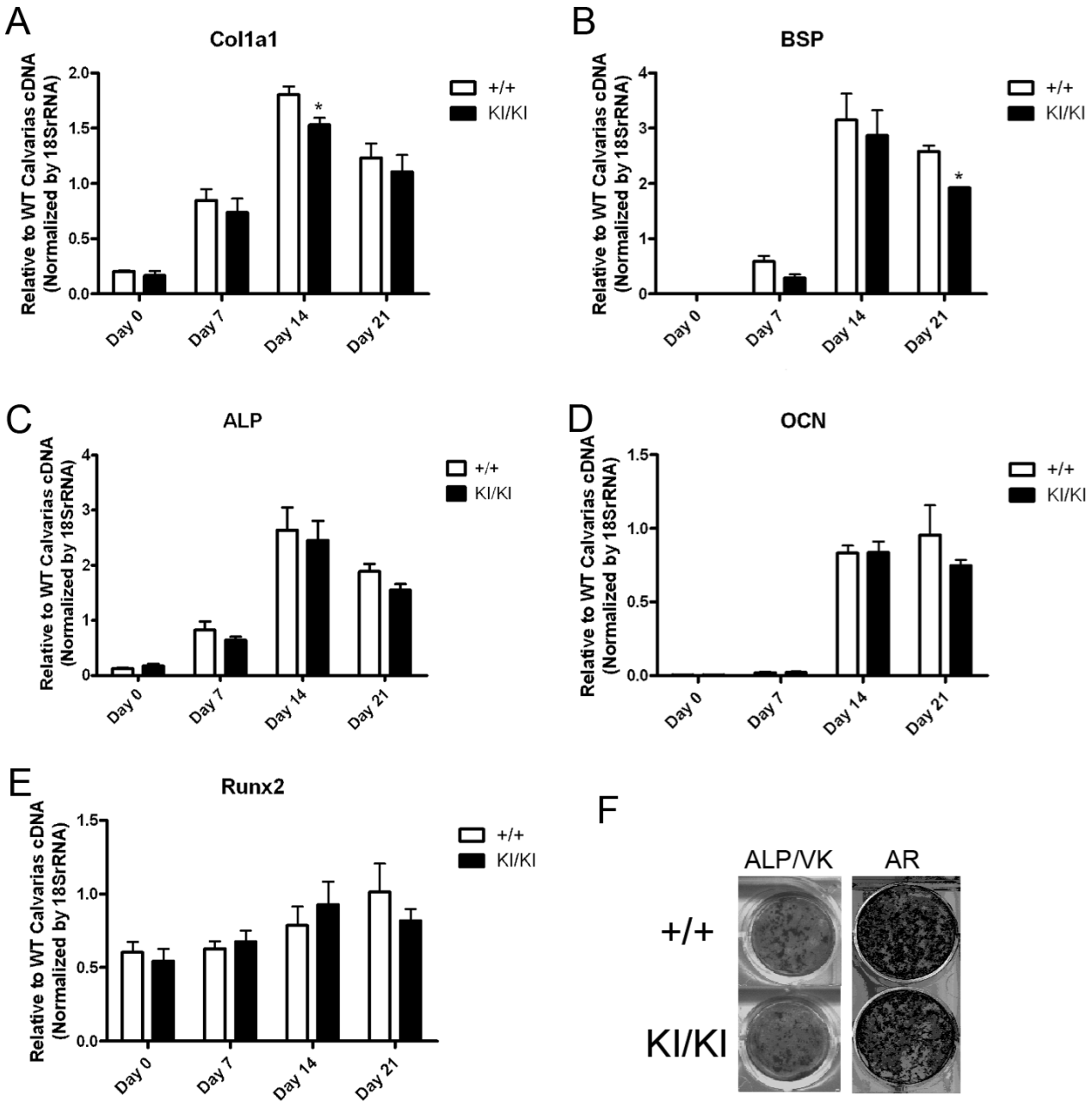

Fig. 5.

Impaired maturation of *Sh3bp2*$^{KI/KI}$ osteoblasts. *Col1a1* (A) and *Bsp* (B) expression in *Sh3bp2*$^{KI/KI}$ osteoblasts by quantitative real-time PCR was significantly decreased compared to *Sh3bp2*$^{+/+}$ osteoblast cultures. Gene expression for *Alp* (C), *Ocn* (D), *Runx2* (E) in late/mature-stage cultures only showed a reduced tendency. Three biological repeats with technical triplicates each were performed for each assay. (Two-way ANOVA followed by Bonferroni post-test, n=3, *p<0.05). Alkaline phosphatase (ALP), von Kossa (VK), and alizarin red (AR) (F) staining of calvarial osteoblast cultures indicated reduced osteogenesis in *Sh3bp2*$^{KI/KI}$ cultures.

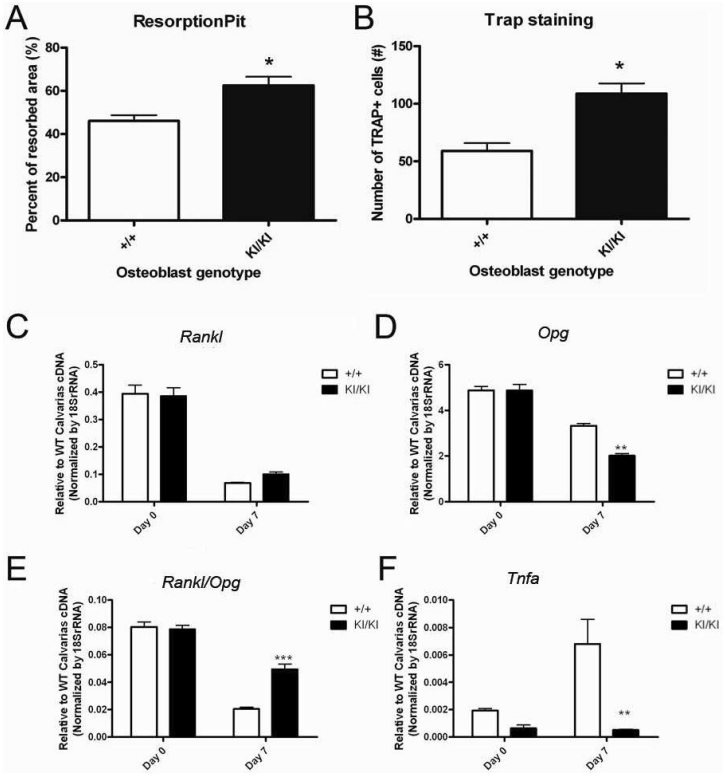

Fig. 6.

Increased osteoclast-inducing potential of *Sh3bp2*$^{KI/KI}$ osteoblasts. *Sh3bp2*$^{+/+}$ bone marrow macrophages were co-cultured with either *Sh3bp2*$^{+/+}$ or *Sh3bp2*$^{KI/KI}$ osteoblasts for 7 days. Bone chip analysis revealed increased resorption activity in co-cultures containing *Sh3bp2*$^{KI/KI}$ osteoblasts (Student's t-test, n=15 for resorption pit; n=6 for TRAP staining; *p<0.05) (A&B). The *Rankl*/*Opg* ratio in osteoblast cultures was significantly higher (with increase in RANKL and decrease in OPG expression) in *Sh3bp2*$^{KI/KI}$ cultures compared to *Sh3bp2*$^{+/+}$ cultures at day 7 of osteoblastic differentiation, indicating an enhanced ability to generate osteoclasts (C–E). The expression of TNF-α in osteoblasts was significantly reduced in *Sh3bp2*$^{KI/KI}$ cultures (F). Biological as well as technical triplicates were performed for each assay. (Two-way ANOVA followed by Bonferroni post-test, n=3, *** p<0.001, ** p<0.01)).

Table 1

Calculated FTIRI parameters of wild-type (Sh3bp2$^{+/+}$) and cherubism (*Sh3bp2*$^{KI/KI}$) mouse bone

Cortical Bones

Sh3bp2 Genotype	**+/+**	**KI/KI**	**↑/↓/NS**
Mineral:Matrix	6.336±0.421	5.568±0.482*	↓
Carbonate:Phosphate ($\times10^{-2}$)	1.003±0.046	1.045±0.051	NS
Carbonate:Amide I ($\times10^{-2}$)	6.360±0.599	5.826±0.681	NS
Crystallinity	1.155±0.012	1.111±0.022*	↓
XLR	2.434±0.115	2.594±0.069*	↑

Trabecular Bones

Sh3bp2 Genotype	**+/+**	**KI/KI**	**↑/↓/NC**
Mineral:Matrix	4.033±0.339	3.425±0.487*	↓
Carbonate:Phosphate ($\times10^{-2}$)	0.849±0.072	0.856±0.076	NS
Crystallinity	1.081±0.017	1.063±0.035	NS
XLR	2.259±0.088	2.480±0.169*	↑

Numbers represent mean and SD for all bones examined

Student's t-test

n=5–6

↑= higher

↓= lower

NS= non significant difference in *Sh3bp2*$^{KI/KI}$ bones

* $p<0.05$